ORIGINAL ARTICLE

Activated-hydrochar derived from olive mill wastes for the removal of phenolic compounds from olive mill wastewater

Ghizlane Enaime[1] · Widad El Bouaidi[2] · Mehdi Louarrat[3] · Abdelaziz Baçaoui[3] · Abdelrani Yaacoubi[3] · Mohammed Loudiki[2] · Marc Wichern[1] · Manfred Lübken[1]

Abstract

In the present study, high-quality activated carbons (ACs) were prepared from a mixture of olive stones and olive mill wastewater (OMWW) through successive hydrothermal carbonization (HTC) and potassium hydroxide (KOH) activation. Textural, morphological, and chemical characteristics of hydrochar (HC) and derived ACs, produced using two KOH/HC ratios (2 and 4), were investigated. KOH activation improved the porous structure of HC and its surface functionality. The best properties were obtained for HC activated by KOH at a ratio of 2 exhibiting a promising surface area ($\approx$1000 m^2/g) and high adsorptive properties towards methylene blue and iodine (617 and 1203 mg/g, respectively). Batch tests were performed to explore the ability of the produced ACs in removing phenolic compounds (PCs) from OMWW, while investigating the effect of contact time, pH, and PCs initial concentration on the adsorption process. The higher removal efficiency was obtained at a pH of 10 after ~ 4 h of contact time. The adsorption kinetic data are well described by the pseudo-second-order kinetic model, while the isotherm adsorption data were found to fit both Langmuir and Freundlich isotherm models. HTC of olive mill wastes followed by KOH activation could be a promising method to produce AC with high porosity and promising potential to remove PCs from OMWW.

Keywords Olive mill wastewater · Olive stones · Hydrothermal carbonization · Hydrochar · Activated carbon · Phenolic compounds

1 Introduction

Activated carbon (AC) is a solid material characterized by an extensive specific surface area, a developed porosity, and a high adsorption capacity toward pollutants, which allows its use in a wide range of industrial and environmental applications. The use of agricultural by-products, as a low-cost and available biomass for AC production, is a promising way for their management bringing benefits with respect to economic, social, and environmental considerations [1, 2]. Pyrolysis and/or gasification are conventionally used as thermochemical processes applied to convert biomass into AC with enhanced physicochemical properties and high adsorption capacity. A pre-drying step is, however, required before pyrolysis to remove moisture from the starting biomass [3]. Alternatively, hydrothermal carbonization (HTC) has recently received increasing attention due to its efficiency to convert wet biomass into a carbon-rich residue, referred to as hydrochar (HC), at relatively high yields by involving a series of simultaneous reactions, including hydrolysis, dehydration, decarboxylation, aromatization, and recondensation [4, 5]. During HTC reaction, biomass is treated at temperatures varying from 180 to 250 °C and under sufficient pressure to keep water in the liquid form [6]. At these conditions, described as the subcritical water medium, the physicochemical properties of water change significantly; the dielectric constant of water becomes much lower than at ambient temperature, making water comport

✉ Ghizlane Enaime
ghizenaime@gmail.com

1 Institute of Urban Water Management and Environmental Engineering, Ruhr-Universität Bochum, Universitätsstraße 150, 44801 Bochum, Germany

2 Laboratory of Water, Biodiversity and Climate Change, Faculty of Sciences Semlalia, Cadi Ayyad University, 40000 Marrakech, Morocco

3 Laboratory of Applied Chemistry and Biomass, Faculty of Sciences Semlalia, Cadi Ayyad University, 40000 Marrakech, Morocco

as a non-polar solvent, which enhances hydrolysis [7, 8]. As compared to high-temperature thermochemical processes, HTC operating at relatively low temperatures is characterized by lower activation energy exhibited during hydrolysis reaction, which could be due to the effect of the subcritical water medium that provide a unique medium for hydrolysis to efficiently convert the lignocellulosic compounds of the feedstock into hydrochar [9, 10]. In addition to the low reaction temperature, HTC processes operate at a short time and a reduced equilibrium moisture content, making HTC the most sustainable conversion technique adapted to seasonal and wet wastes [11, 12].

Many applications of HC have been proposed including its use as a solid biofuel [13] and as a soil amendment to improve soil properties and promote long-term carbon storage [14]. HC may also be explored as an adsorbent in removing pollutants in different environmental applications [15]. However, owing to its low content in functional groups and less developed surface area and porosity, a subsequent activation of HC via chemical or physical methods is necessary [16]. Chemical activation using KOH as an activating agent is a well-known strategy to produce highly porous carbon materials; its application to hydrothermal carbons has been previously investigated [1, 17–19]. Many variables involved in the KOH activation process are reported affecting the final AC properties, where the nature and origin of precursor, the activation temperature, and the KOH/HC ratio were selected as the most important ones. The activation temperature is largely studied and optimized to enhance the textural structure of the produced AC and its adsorption capacity [20, 21]. As previously discussed by Wu et al. [19], the reaction between KOH and carbon requires high energy. At low temperature (600 °C), only a small pore size and low surface area could be produced due to the incomplete reaction. At temperatures ranging from 700 to 800 °C, the reaction becomes more violent, leading to more pore formation and enhancement of AC surface area. Increasing the activation temperature up to 900 °C causes the collapse and destruction of pores and due to the severe thermal treatment; mesopores may increase while the surface area decreases [1, 22]. Regarding the effect of KOH/HC ratio, it has been reported as the crucial parameter involved in the chemical activation process, and hence, it is widely used as variable to enhance the adsorption capacity of AC prepared from different kind of starting precursors [23].

Chars from olive mill wastes (OMWs) and their derived ACs have been widely applied as adsorbents of several organic and inorganic contaminants [24]. Due to the high performance, increased research effort has recently performed to properly implicate OMW-derived sorbents in the treatment process of OMWW, in accordance with the concept of circular economy. An integrated and innovative process has been conceived by Abid et al. [25] aiming at the development of a cost-effective and sustainable approach for the detoxification of OMWW. Authors proceed to the pyrolysis conversion of olive mill solid wastes into biochar, which was then used to remove phenolic compounds (PCs) from OMWW. A removal efficiency of 63.16% has been reported under optimal conditions of pH 12, initial PCs concentration of 680 mg/L, adsorbent dosage of 15 g/100 mL, and pyrolysis temperature of 650 °C. AC produced by physical activation of olive pomace has also been successfully used for PCs sorption [26].

Interestingly is the valorization of both solid and liquid OMWs in one stream to produce AC and its use as an adsorbent to remove PCs from OMWW. In the present study, AC was produced via successive HTC of a mixture of olive stones (OS) and OMWW and chemical activation of the produced HC using KOH as an activating agent at two different KOH/HC ratios. The HC and the HC-derived ACs were systematically characterized by thermogravimetric analysis (TG/DTG), Fourier transform infrared spectroscopy (FTIR), scanning electronic microscopy (SEM), elemental analysis CHNO, ultimate analysis, BET analysis, and MB and iodine adsorption tests. The adsorption of PCs on the OMW-derived ACs was investigated, and the effect of different parameters such as contact time, OMWW, initial pH, and initial PCs concentration were assessed. Pseudo-first-order and pseudo-second-order models have been used to study the adsorption kinetic of PCs on ACs, while the prediction of the PCs adsorption was performed using the nonlinear Langmuir and Freundlich isotherm models.

2 Experimental

2.1 HC preparation

The raw material as employed consisted of a mixture of OS and OMWW. OS were provided by an olive oil production cooperative located in Marrakech-Morocco performing a system to separate crushed OS from the two-phase olive mill waste. In this study, the fraction of OS with a particle size between 2 and 3.15 mm was used. The main characteristics of OS are 24.7% fixed carbon, 70.5% volatile matter, 2.3% ash, 19.7% hemicellulose, 17.8% cellulose and 37.8% lignin. The used OMWW had values of PCs, chemical oxygen demand and total suspended solids of 3.4 g/L, 120 g/L and 5 g/L, respectively.

HTC experiments were carried out in a Prolabo 0.125-L non-stirred pressure reactor, equipped with a PID controller and a pressure gauge. A known mass of OS mixed with OMWW at a liquid/solid ratio of 60% (w:w) was introduced into the reactor and the autoclave was heated from the room temperature to the set point 260 °C and hold at this temperature for 4.5 h. After cooling down, HC was separated from

the liquid suspension by vacuum filtration, washed with distilled water, and dried at 105 °C for 24 h.

2.2 HC activation

The chemical activation of the produced HC was carried out using KOH (85–100.5% pure, 56.11 g/mol; Sigma-Aldrich) as an activating agent at two KOH/HC weight ratios; 2 and 4. The activation method is similar to that used by Ubago-Perez et al. [27] with few modifications. Initially, a known mass of HC was immersed in a KOH solution; the mixture was stirred for 2 h at 60 °C and dried at 105 °C until total evaporation. The impregnated and dried HC was placed into the reactor, which was then heated to 800 °C at a rate of 10 °C/min and kept for 1-h holding time under nitrogen flow (300 mL/min). After activation, the heating was turned off allowing the sample to cool down. The resulting carbon was washed thoroughly using 1N HCl (37%; Carlo Erba) to remove the inorganic matter, followed with hot-water washing until the water pH became neutral. The washed carbon was then dried at 105 °C and stored before analysis. The resulting AC samples are denoted as HC-AC-KOH2 and HC-AC-KOH4, where KOH2 and KOH4 correspond, respectively, to KOH/HC activation ratios of 2 and 4.

2.3 Characterization

The adsorption capacity of ACs towards iodine (99.5–100.5% pure, 253.81 g/mol; VWR, Germany) was determined using sodium thiosulfate (99.5%, 248.18; Riedel-de Han) volumetric method [28], while the capacity of ACs to adsorb MB ($\geq$ 97.0% pure, 319.85 g/mol; Sigma-Aldrich) was evaluated by spectrophotometric method at the maximum absorbance wavelength 660 nm [29]. Thermal gravimetric analysis (TGA) and its derivative (DTGA) were performed using a thermo-gravimetric analyzer (Labsys Evo TGA); TGA was performed by heating the HC sample at a rate of 10 °C/min to a temperature of 950 °C under an inert atmosphere. The surface morphology of the feedstock, HC, and ACs was examined by Philips XL-30 scanning electron microscopy, while the analysis of surface functional groups of samples was carried out using FTIR on a PerkinElmer spectrometer. Elemental analysis was carried out using an Elemental Analyzer Vario EL 3 instrument. The BET surface area (S_{BET}) was determined by analyzing nitrogen adsorption/desorption isotherms at 77 K using Autosorb 1 from Quantachrome and its value was obtained from the isotherms using Brunauer–Emmett–Teller (BET) model. The total pore volume (V_T) was obtained from the specific adsorption of N_2 at a $p = p_0 = 0.95$. The micropore volume (V_{mic}) and the mean micropore width (L_0) were determined using the Dubinin-Radushkevich equation applied to N_2 adsorption data. The concentration of PCs before and after adsorption was determined by Folin-Ciocalteu technique at 760 nm [30].

2.4 Adsorption experiments

Batch experiments were performed to assess the performance of the prepared ACs in removing PCs from OMWW. 2 g of each AC sample was introduced into a 150-mL conical flask containing 100 mL of decanted OMWW with a concentration of total PCs equal to 50 mg/L. For the kinetics study of PCs adsorption onto ACs, the mixture was agitated at 150 rpm at predetermined times (0.5, 1, 1.5, 2, 3, 4, 8, 24 h) using a rotary shaker. At the end of each experiment, the samples were filtered using a 0.45-µm filter, and the filtrates were analyzed for residual PCs concentration. Univariate experiments were also performed to evaluate the effect of OMWW initial pH (2–10) on the PCs removal. The effect of PCs initial concentration on the ACs' adsorption capacity was investigated by using different initial PCs concentrations (50, 100, 200, 300, 400, and 500 mg/L). After equilibrium time, determined by kinetic study, samples were filtered and analyzed for residual PCs concentration.

The AC adsorption capacity (Q_e) was calculated using Eq. (1):

$$Q_e = \frac{(C_0 - C_e) \times V}{m} \quad (1)$$

where C_e and C_0 are the equilibrium and the initial concentration (mg/L) of PCs, respectively; m (g) is the amount of AC; V (mL) is the volume of OMWW.

To investigate the best-fit model for the adsorption kinetic, non-linear forms of pseudo-first-order and pseudo-second-order kinetic models have been used. In the pseudo-first-order model Eq. (2), it is assumed that the rate of adsorption is proportional to the concentration of adsorbate [31]:

$$Q_t = Q_e \left[1 - e^{-k_1 t} \right] \quad (2)$$

where Q_e is the equilibrium adsorption capacity (mg/g), Q_t is the adsorption capacity at time t (mg/L), and k_1 is the pseudo-first-order rate constant (min^{-1}).

The pseudo-second-order model, represented by Eq. (3), is based on the assumption that the adsorption is mainly controlled by chemisorption mechanism [32]:

$$Q_t = \frac{k_2 Q_e^2 t}{1 + k_2 Q_e t} \quad (3)$$

where Q_e is the equilibrium adsorption capacity (mg/g), Q_t is the adsorption capacity at time t (mg/g), and k_2 is the pseudo-second-order rate constant (g/mg min).

Experimental date corresponding to the adsorption of PCs on ACs were analyzed using Langmuir and Freundlich isotherm models. Langmuir isotherm model, represented by Eq. (4), assumes that adsorbate is forming a monolayer on surface of adsorbent exhibiting a finite number of homogenous sorption sites [33]:

$$Q_e = \frac{Q_m k_L C_e}{1 + k_L C_e} \tag{4}$$

where k_L is the Langmuir constant indicating to the strength of interaction between adsorbate and adsorbent surface and Q_m is corresponding to the maximum adsorption capacity of ACs.

Unlike Langmuir model, Freundlich equation (Eq. (5)) is generally used for multilayer adsorption on adsorbents with heterogeneous sites [34]:

$$Q_e = k_F C_e^{\frac{1}{n_F}} \tag{5}$$

where Q_e is the equilibrium adsorption capacity (mg/g), C_e is the equilibrium concentration of PCs (mg/L), and k_F and $1/n_F$ are the Freundlich constants corresponding, respectively, to bonding energy and heterogeneity factor.

3 Results and discussion

3.1 Characterization of HC and HC-derived ACs

3.1.1 TG-DTG analysis of HC

Thermal decomposition behavior of HC was investigated by thermo-gravimetric analysis. The TGA and its derivative (DTGA) profiles are shown in Fig. 1. The slight mass loss at temperatures < 120 °C was accounted for the evaporation of water and volatilization of small organic molecules [35]. Two main regions of weight loss were distinguished in a temperature range from 202 to 737 °C. The first weight loss (around 4%) observed between 202 and 343 °C, whose peak centered at approximately 290 °C (T_1), is may be attributed to the degradation of re-polymerization products formed during the HTC at high temperature [35]. The second peak, observed at temperatures between 343 and 744 °C, with a maximum weight loss (32%) at 435 °C (T_2), corresponds to the main stage of the mass loss, and it is mainly related to the degradation of lignin. Thus, the HTC of the mixture of OS and OMWW at the experimental conditions led to the degradation of both hemicellulose and cellulose and probably to the re-polymerization of primary degradation products at high temperature.

3.1.2 Surface chemistry characterization

The FTIR spectra of raw feedstock and HC (Fig. 2), highlighting the chemical transformations during the thermal process, revealed that noteworthy changes occurred during the HTC treatment of OMWs and the subsequent activation of HC. After heating the feedstock at 260 °C during 4.5 h, the intensities of bands at 1041 cm^{-1} and 3462 cm^{-1}, attributed to O–H stretching vibrations in hydroxyl groups and/or carboxyl groups, were decreased most likely due to the reaction of dehydration of raw feedstock. Band at 1248 cm^{-1} may be attributed to esters (e.g., R-CO–O-R'), ethers (e.g., R-O-R'), or phenol groups [36] and at 1450 cm^{-1} (indicator of residual lignin), corresponding to aromatic C = C, was
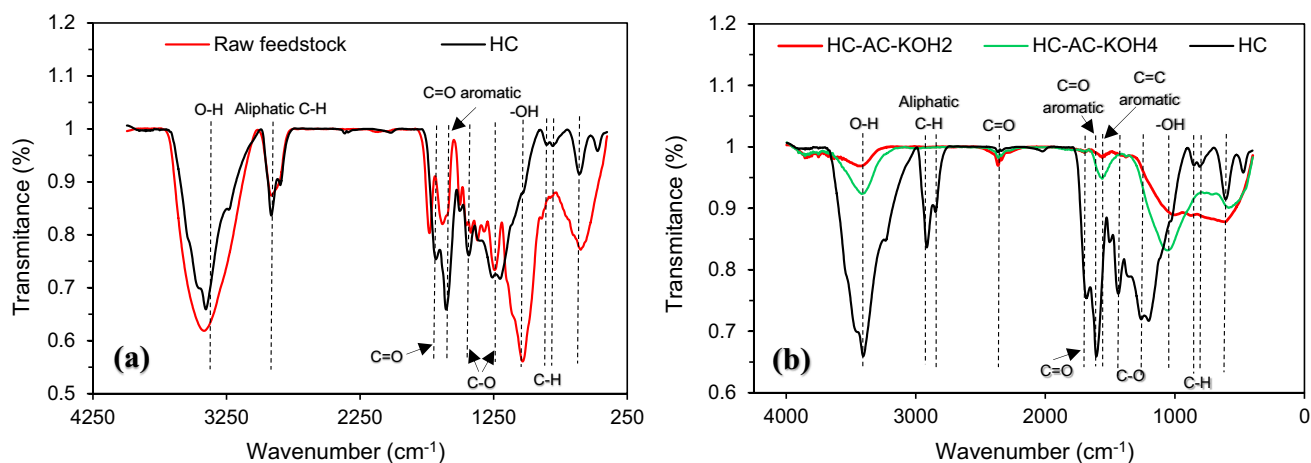
Fig. 1 TGA and DTGA curves of HC
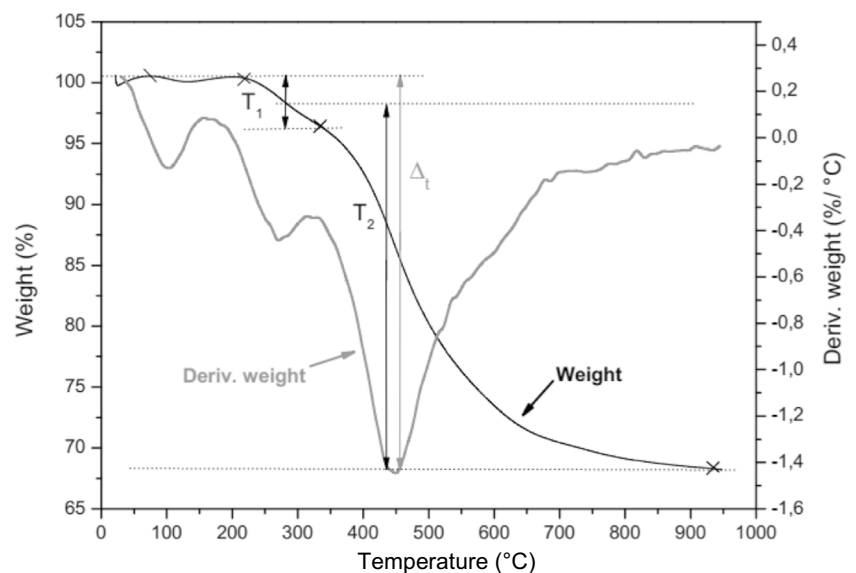
Fig. 2 FTIR spectra of **a** feedstock and HC and **b** HC, HC-AC-KOH2, and HC-AC-KOH4

slightly increased. The aromatization reactions occurred during HTC were evidenced by the band at 1620 cm^{-1} ascribed to C = O vibration stretching conjugated to the aromatic ring [37] and evenly provided in the appearance of the bands at 800–870 cm^{-1} corresponding to aromatic C–H [38]. It is shown that the intensity of the band at 1700 cm^{-1}, assigned to C = O vibrations corresponding to carbonyl, quinone, ester or carboxyl, was gradually increased. The FTIR spectra of HC shows (in relation to the raw) a slight increase in the band intensity observed at 3000–2800 cm^{-1} due to stretching vibrations of aliphatic C–H. During the HTC treatment, most of hemicellulose and water-soluble organic compounds are dissolved in the liquid phase. Thus, the detected functional groups on HC surface are corresponding to cellulose and lignin components and some transformation products [39]. The activation of HC leads to more chemical transformations. The FTIR spectra of HC compared to carbons chemically activated by KOH are shown in Fig. 2. The analysis of FTIR spectra revealed that the band at 3400 cm^{-1}, attributed to OH stretching, was dramatically diminished after activation, especially for HC-AC-KOH2. Moreover, for both ACs an intense band near 1100 cm^{-1} was distinguished which means the apparition of secondary hydroxyl groups. We observed also a complete disappearance of the band at 3000–2800 cm^{-1} and the band at 1700 cm^{-1}, while the intensity of the band observed at 2355 cm^{-1}, corresponding to the C = O stretches of ambient CO$_2$ molecules [40], was slightly increased. The greater aromatic C = O band observed at 1600 cm^{-1} for HC was dramatically diminished after activation. It is worth noting that this band was overlap with the band at 1514 cm^{-1} corresponding to the aromatic C = C vibration, which explains the appearance of a wide band in the region between 1500–1600 cm^{-1}

after activation. A sharp decrease of bands observed at 1440 and 1366 cm^{-1} was also noticed, whereas the bands observed at 1250 cm^{-1} and at 800–870 cm^{-1} are completely disappeared.

3.1.3 Surface morphology characterization

The SEM images, illustrated in Fig. 3, show that the morphologies of the precursor, HC, and ACs were quite different. In the precursor, it could be observed that the particles were highly packed, while the morphology of the HC exhibited a regular structure with some pores detected on the surface rearranged and opened up as a consequence of the hydrothermal dissolution/decomposition reactions and volatile organic substances release [41, 42]. As compared to the HC, KOH-activated HC exhibited morphology with well-developed porosity. Activation using alkali metals such as KOH involves oxidation–reduction reactions, which allow the creation of porosity. These reactions are strongly affected by the surface properties of the precursor. Falco et al. [17] showed that a raise in the HTC temperature from 180 to 240 °C leads simultaneously to an increase in the content of oxygen functional groups on the surface of hydrothermal carbons, which may help increasing the accessibility of KOH molecules to the interior of HC and creating more porosity. Increasing the HTC temperature beyond 280 °C allows generating a higher aromatized HC with high stability and structural order, which reduced the HC reactivity and lead to reduced porosity development. The increase in the KOH/HC ratio from 2 to 4 also promoted a relatively opening of pores. KOH/HC ratio is a decisive parameter that strongly affect the formation of pores. KOH intercalates between carbon layers and decompose into more active components, allowing the destruction of aromatic layers and the creation of more porosity [43]. At higher KOH addition, the severity
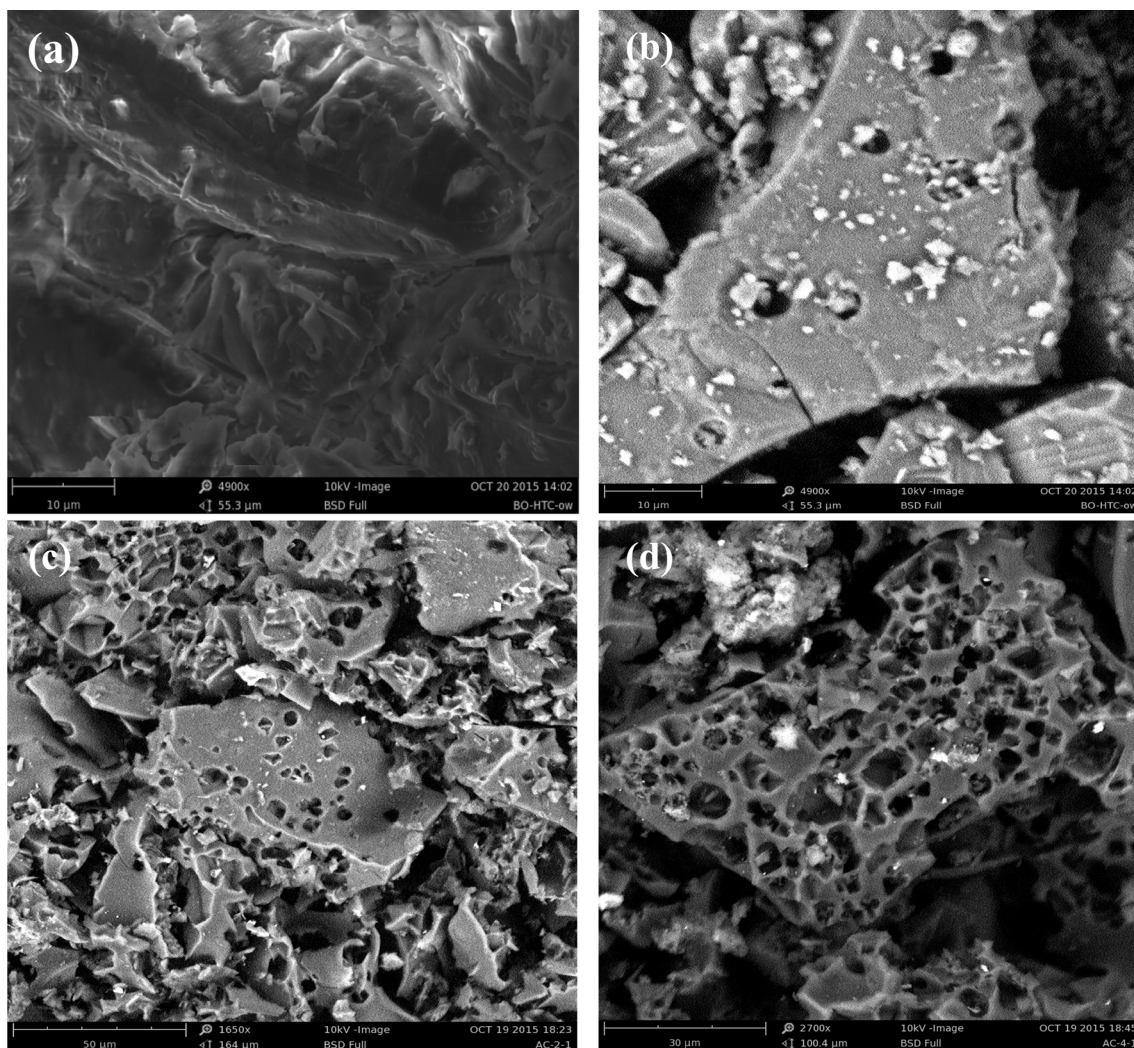
Fig. 3 SEM images of **a** raw feedstock, **b** HC, **c** HC-AC-KOH2, and **d** HC-AC-KOH4

of KOH reaction with carbon increased due to the acceleration of reaction rate and the increase in catalytic oxidation, which causes the widening of the preexisting pores. Moreover, KOH molecules added at excessive amount might also decomposed into water which causes gasification reactions leading to more widening of pores [44]. As shown in Fig. 3, the HC-derived AC is exhibiting a roughly surface due to

the heterogeneity of pores in its structure, which could be advantageous to retain more polluting molecules.

3.1.4 Elemental analysis

The elemental composition of feedstock, HC, and derived ACs are summarized in Table 1. As can be seen, the

Table 1 Elemental composition of feedstock, HC, and HC-derived ACs

Materials	C (wt%)	H (wt%)	N (wt%)	Oᵃ (wt%)	H/Cᵇ	O/Cᵇ
Raw feedstock	48.3	6.4	0.2	45.0	1.59	0.70
HC	77.1	5.6	1.9	15.5	0.87	0.15
HC-AC-KOH2	77.8	0.9	1.6	19.6	0.14	0.19
HC-AC-KOH4	78.8	1.0	1.5	18.6	0.16	0.18

ᵃCalculated by difference

ᵇAtomic ratios

composition of raw OMWs changed markedly after HTC treatment. As expected, the carbon content increased from 48.3 wt% in the feedstock to 77.1 wt% in the HC, and the oxygen and hydrogen contents were decreased after carbonization from 45 to 15.5 wt% and from 6.4 to 5.6 wt%, respectively. The presented carbon content is higher than those reported by others [3, 45, 46]. As compared to HC, the elemental analysis of both HC-derived ACs exhibited similar values of carbon content regardless of the activation ratio (Table 1). An increase in the oxygen content was however observed after HC activation, this can be due to the high degree of surface oxidation, a phenomenon typically observed after KOH activation [47]. The same tendency was also observed by de Araújo et al. [48] and Yu et al. [49]. The H/C and O/C atomic ratios were calculated for raw feedstock, HC and derived ACs and their values are summarized in Table 1. At experimental HTC conditions, a loss of oxygen and hydrogen contents, expressed respectively by a decrease in H/C and O/C atomic ratios from 1.59 to 0.87 and from 0.70 to 0.15, was observed. Under HTC conditions, the reduction of hydrogen and oxygen corresponds in principle to ongoing dehydration and demethylation (loss of CH_3) and/or decarboxylation (loss of CO_2) reactions [50]. The atomic ratios of elements corresponding to HC-derived ACs are also shown in Table 1. The H/O ratio of HC was decreased markedly after KOH activation from 0.87 to 0.14–0.16, while the O/C ratio was increased from 0.15

to 0.18–0.19, following an increase in the oxygen content after KOH activation as previously described.

3.1.5 Textural characteristics of HC-derived ACs

Figure 4 shows the N_2 adsorption–desorption isotherms at −196 °C and the pore size distribution of HC-AC-KOH2 and HC-AC-KOH4, while Table 2 collects the main characteristics relative to the porous texture of both HC-derived ACs.

Both HC-derived ACs showed isotherms type I according to the classification by IUPAC characteristic of microporous materials, with remarkable N_2 adsorption at low relative pressures and a minor contribution of mesoporosity [49, 51], as confirmed by the low values of the S_{EXT}, the high V_{mic} values and the average pore size of about 2 nm (Table 2). A higher surface area (964 m^2/g) and pore volume (0.51 cm^3/g) have been exhibited by HC-AC-KOH2 as compared to HC-AC-KOH4 showing 890 m^2/g BET surface area and 0.47 cm^3/g pore volume (Table 2). The relatively high values of HC-AC-KOH2 surface area and pore volume could be compared with those of commercial ACs provided by Calgon Corporation, such as F100 and BPL showing values of BET surface area of 957 and 972 m^2/g and total pore volume of 0.526 and 0.525 cm^3/g, respectively [52]. A KOH/HC ratio of 2 was also reported as optimum by Shen et al. [53] and Abdel-Ghani et al. [54]. The yield as also shown in Table 2 varies, however, in the opposite trend and increases from 25 to 28% as the KOH/HC ratio increases, the fact that
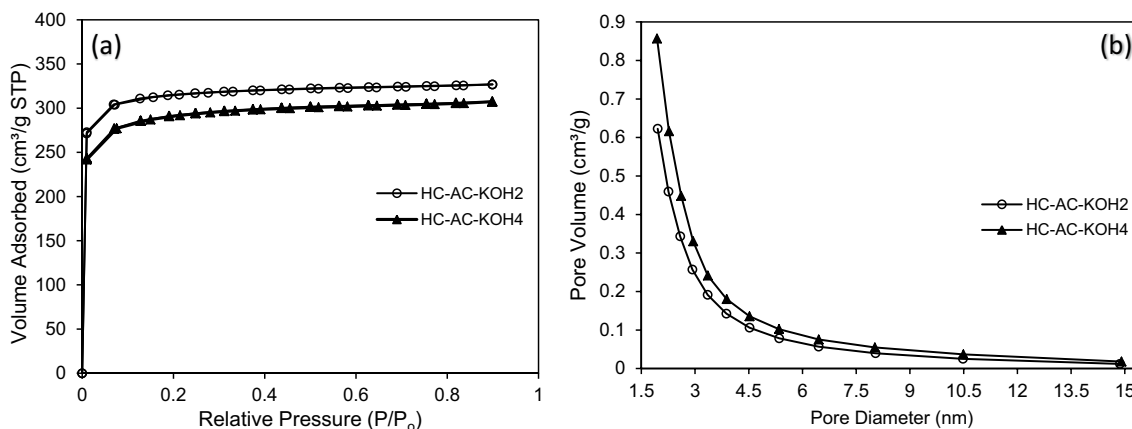

Fig. 4 **a** N_2 isotherms at 77 K and **b** pore size distribution of HC-AC-KOH2 and HC-AC-KOH4

Table 2 Textural properties of HC-derived ACs

Materials	Mass yield*	MB adsorption	I$_2$ number	S$_{BET}$	S$_{mic}$	V$_T$	V$_{mic}$ (N$_2$)	L$_0$ (N$_2$)
	(%)	(mg/g)	(mg/g)	(m^2/g)	(m^2/g)	(cm^3/g)	(cm^3/g)	(nm)
HC-AC-KOH2	25	617	1203	964	865	0.51	0.44	2.10
HC-AC-KOH4	28	579	1022	890	746	0.48	0.39	2.14

*AC yield is calculated based on the mass of the starting biomass on a dry basis

surface area depends on the mass removed during the activation process, which allows creating pores in the structure of material and improves its specific surface area. The effect of KOH/HC ratio on mass yield and ACs surface area can be explained by the mechanism proposed by Tseng et al. [55], bringing out two possible reactions that can be implicated during KOH activation: physical surface pyrolysis and chemical KOH etching. According to Tseng et al. [55], both reactions interfere in the activation process when the KOH/HC ratio is low, which explain the high surface area, whereas, at high KOH/HC ratio (KOH/HC ratio higher than 4), the physical surface pyrolysis is interrupted due to the relatively high coverage of KOH onto HC which promoted the KOH etching. In previous studies, KOH/HC ratio was reported as the most important activation parameter playing a crucial role in the formation of pores [19, 56]. KOH reacts with HC-forming K_2CO_3 and leading to the formation of pores and to the increase in the surface area [44]. However, El-Hendawy [57] observed that a high KOH/HC ratio might lead to a high formation of K_2CO_3 and metallic potassium, which persist in the carbon structure and cannot be easily leached off even after repeated washing. The excess of K_2CO_3 and metallic potassium may block some pores and therefore decreases the AC surface area. The effect of KOH/HC ratio (from 1 to 4) on pore formation within AC prepared at 800 °C was studied by Wu et al. [19]. Authors reported that at relatively low KOH/HC ratio, the formation of pores is generally attributed to the opening of previously inaccessible pores and to the formation of new pores. By increasing the KOH/HC ratio (over 3), an expanding of the existing pores may take the dominance in the reaction, which causes a large pore size.

As previously reported by [17] and [58], the HTC pretreatment of biomass has a homogenizing effect, allowing the removal of undesirable mineral matter from the carbonaceous material. A successive activation of the produced biochar leads to an intensive release of VM as gases, which creates pores in the overall structure of the derived-AC and significantly increases its surface area. Such a porosity enhancement could also be recognized from the examination of MB and iodine adsorption. The values of MB and iodine adsorption capacities are also shown in Table 2. The MB value, defined as the number of mg of standard MB molecule in aqueous solution removed by 0.01 g of AC, gives an indication of the development of porosity of carbons. As shown in Table 2, the KOH-R2-AC showed the higher MB adsorption capacity as compared to the KOH-R4-AC, since it presents the higher specific surface area and pore volume. This value is considerably higher than the values reported in the literature for AC prepared by successive HTC and sodium hydroxide activation [39] and commercial AC (Calgon Filtrasorb) [59]. The iodine number expressed as milligrams of iodine per gram of adsorbent is a quick test to

have a good simulation of the internal surface area [60]. The KOH-ACs showed values of iodine number ranging from 1022 to 1203 mg/g; these high values confirm the developed microporous structure exhibited by both carbons. The highest iodine adsorption (1203 mg/g) was afforded by the KOH-R2-AC, which is higher than another AC prepared by HTC followed by KOH activation [1].

3.2 Phenolic adsorption experiments

3.2.1 Kinetic adsorption

Kinetic study is a useful method to evaluate the rate and mechanism controlling the adsorption process. As can be seen in Fig. 5, the rate of PCs adsorption on both ACs was high at the initial contact time up to 2 h and then gradually reduced until achieving the equilibrium (~4 h), where no more PCs are further removed from OMWW. Galiatsatou et al. [26] reported that the equilibrium of OMWW-PCs adsorption onto AC produced from olive pulps and OS could be achieved between 1 and 22 h. The two-step adsorption is typically observed during the adsorption of contaminants on AC. The first step characterized by a rapid uptake of PCs is generally occurred in mesopores within the external surface, while the second one is corresponding to a microporous diffusion and is characterized by a slow adsorption rate probably related to slow pore diffusion of adsorbate into the bulk of the adsorbent [61, 62]. The relatively rapid PCs adsorption observed during the first 2 h indicates that more than one mechanism might be involved in PCs adsorption process. As shown in Fig. 5, about 28 to 31% of total PCs were removed at equilibrium. A relatively higher removal efficiency (between 38 and 40%) of PCs from OMWW was reported by Senol et al. [62] after 2 h of adsorption using a commercial AC. The similar removal efficiency was also obtained by Aliakbarian al. [63] but after a contact time of only 10 min.
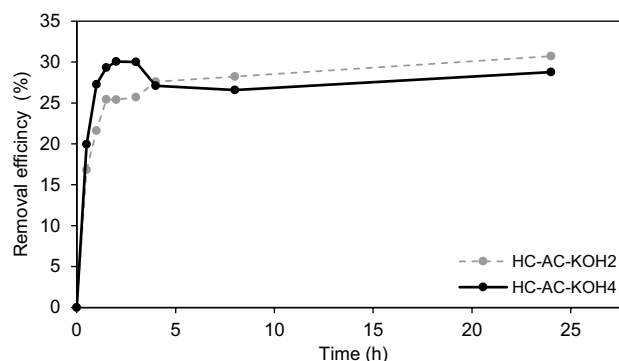

Fig. 5 Effect of contact time on PCs removal from OMWW (Initial PCs concentration = 50 mg/L) using 2 g of AC in 100 mL of solution

The adsorption rate indicates the time required for reaching equilibrium of the adsorption process. In the present study, the potential rate and mechanism controlling the PCs adsorption process were evaluated using the pseudo-first-order and pseudo-second-order models. Calculated rate-controlling constants pertaining to both kinetic models and the amount of PCs uptake at equilibrium for both AC samples are presented in Table 3. The suitability of the pseudo-first and pseudo-second-order models to fit the kinetic data corresponding to the adsorption of PCs on the two ACs was evaluated by comparing the values of their corresponding correlation coefficients (R^2). For both AC samples, the pseudo-second-order model leads to higher fitting quality based on its higher R^2 values as compared to that corresponding to the pseudo-first order model (Table 3). Additionally, only a slight difference was observed between the experimental and the predicted adsorption data, confirming the applicability of the pseudo-second-order model to describe the adsorption process. Similar findings were also reported by Aliakbarian et al. [63] and Abid et al. [25] during the adsorption of PCs onto biochar and commercial AC, respectively. Accordingly, it could be assumed that chemical adsorption could be the dominant rate-controlling step for the adsorption of PCs on both AC samples [2]. The main mechanisms involved in the adsorption process could be controlled by exchange reactions between PCs and functional groups on AC surface until saturation of all adsorption sites. Afterward, other interactions such as hydrogen bonding could be involved in the adsorption process.

3.2.2 Effect of pH

To investigate the effect of OMWW initial pH on PCs removal, a series of experiments was carried out using a diluted OMWW (initial PCs concentration, 50 mg/L) at various pH values ranging from 2 to 10. The obtained results are summarized in Fig. 6.

For HC-AC-KOH2, only slight changes in PCs removal were observed when the pH raised from 2 to 8, while an important increase was recorded at pH ranging from 9 to 10. For HC-AC-KOH4, total phenols removal showed a decreasing trend when the pH increased from 2 to 5 and then gradually increased until reaching its maximum at a pH of 10 (Fig. 6). As previously reported, PCs at a solution pH lower than their pK_a remain undissociated and start to dissociate into anionic forms at pH close or higher than
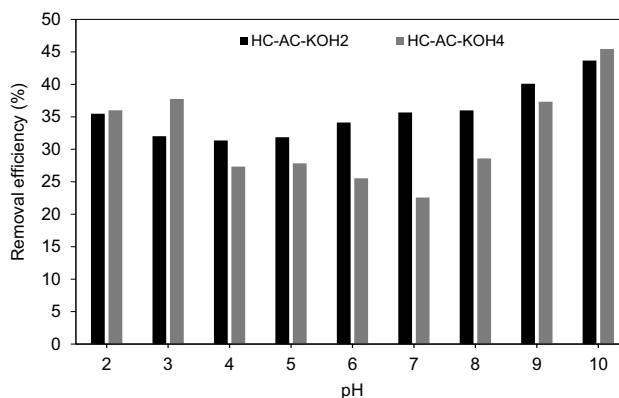

Fig. 6 Effect of OMWW initial pH on the adsorption of PCs on HC-AC-KOH2 and HC-AC-KOH4

their pK_a [64]. However, due to the high variety of PCs present in OMWW and obviously their different pK_a values, it might be difficult, even impossible, to predict the dominance of ionic or neutral forms of PCs in solution, and then the dominating mechanism controlling the adsorption process. According to Stasinakis et al. [65], AC surface functional groups and PCs could be simultaneously present in solution in their protonated and deprotonated forms, giving rise to different surface-PCs interactions to be involved, namely, electron donor–acceptor interactions, dispersion effect between the aromatic phenolic ring and the electrons in carbons and electrostatic attraction and repulsion between AC surface and PCs species [66]. At low pH values, AC surface is generally exhibiting a positive charge; the high adsorption capacity observed at this range of pH could be due to the electrostatic interactions between PCs and the negatively charged groups likely present on the AC surface characterized by its heterogeneity [67]. van der Waals forces and p-p dispersion interactions could also be involved at low pH values, as most of the AC surface is unavailable for the adsorption of co-ionic species [68]. At pHs around 7.0, Romero-Cano et al. [69] reported that the adsorption of PCs is possibly promoted by the formation of hydrogen bonds between the PCs-hydroxyl group and the deprotonated acid sites (R-COOH, R-OH) of the AC. The relatively lower removal efficiency of PCs observed at this range of pH (Fig. 6) could be, however, attributed to the competition between protons introduced by the acid solution of OMWW and the PCs for adsorption sites [70]. At

Table 3 Kinetic parameters for adsorption of PCs onto HC-AC-KOH2 and HC-AC-KOH4

Materials	Q_{exp}	Pseudo-first order			Pseudo-second order		
		Q_{th} (mg/g)	k_1 (min^{-1})	R^2	Q_{th} (mg/g)	K_2 (g/mg.min)	R^2
HC-AC-KOH2	7.50	7.2498	0.0417	0.9989	7.5533	0.0129	0.9997
HC-AC-KOH4	7.68	6.9599	0.0271	0.9913	7.58346	0.00562	0.9999

pH higher than 9, PCs are mostly in the form of phenolates, and the surface of HC-derived ACs would be negatively charged; the higher adsorption capacity observed at this range of pH could be then attributed to hydrogen bonding [20, 55]. It is also expected that electrostatic attraction may occur between PCs and the positively charged groups probably existing on the AC surface at this pH, as also reported by Achak et al. [72].

3.2.3 Effect of initial PCs concentration

Regarding the effect of PCs initial concentration on their removal efficiency, the adsorbed amount of PCs varies proportionally with the increase in initial PCs concentration (Fig. 7), which indicates an increase in the overall AC surface area occupied by PCs and a decrease in the free sites as the aqueous PCs concentration increases. A higher concentration of adsorbate in solution can increase the driving force to overcome the resistance to mass transfer between aqueous and solid phases, which increases the collision probability between adsorbate and adsorbent [73]. The PCs removal efficiency tends, however, to go to a decreasing profile as the initial PCs concentration increases. This could be related to the composition and concentration of some PCs present in the real OMWW. According to some author's assumptions, hydroxytyrosol and tyrosol, present in significantly higher concentration in OMWW, should be adsorbed onto AC sorbent with lower removal efficiency while all other

low-molecular-weight PCs should be almost completely removed [62].

The analysis of the interaction between PCs and AC and the stimulation of the potential mechanisms involved in the adsorption process could be performed by the analysis of adsorption isotherms using theoretical equations such as those corresponding to Langmuir and Freundlich models. The calculated Langmuir and Freundlich constants are shown in Table 4.

As shown in Table 4, both models are exhibiting satisfactory correlation coefficients for both AC samples; the value of R^2 is, however, displaying a privilege to the Freundlich model for both samples. Accordingly, Freundlich model is more suitable to describe PCs adsorption onto both AC samples. The magnitude $1/n_F$ as shown in Table 4 indicates the favorable character of the adsorption process. A value of $1/n_F$ closer to zero indicates greater adsorbent heterogeneity [39]. Langmuir adsorption model assumes a monolayer adsorption at specific homogeneous surface sites, while Freundlich model presumes that the adsorption is not monolayer rather a multilayer adsorption on heterogeneous sites with non-uniform distribution of energy level. Considering the high R^2 values obtained for both models, it could be assumed that both monolayer and heterolayer adsorption may occur due to the AC surface that contained uniformly distributed heterogeneous adsorption sites. The same assumption was also reported by Achak et al. [72] and Abid et al. [25]. When applying the Langmuir model, the maximum PCs adsorption

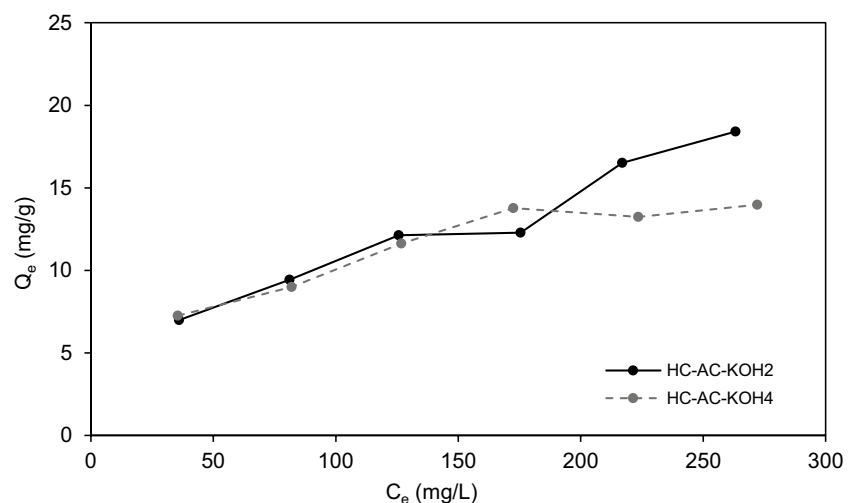**Fig. 7** Adsorption isotherms of PCs on HC-AC-KOH2 and HC-AC-KOH4

Table 4 Langmuir and Freundlich isotherm parameters of PCs adsorption on HC-AC-KOH2 and HC-AC-KOH4

Materials	Langmuir			Freundlich		
	Q_m (mg/g)	k_L (L/mg)	R^2	k_F (mg/g)(L/ mg)$^{1/n_F}$)	$1/n_F$	R^2
HC-AC-KOH2	26.50	0.0070	0.953	0.9636	0.5244	0.991
HC-AC-KOH4	16.88	0.0181	0.996	2.2224	0.3349	0.999

capacity was equal to 26.50 mg/g for HC-AC-KOH2 and 16.88 mg/g for HC-AC-KOH4, which are higher than those obtained with AC physically prepared from solvent extracted olive pulp with Q_{max} of 12.4 mg/g [26] and incompletely combusted olive pomace with Q_{max} of 11.4 mg/g [65]. The higher adsorption capacity of HC-AC-KOH2 as compared to HC-AC-KOH4 could be attributed to its well-developed porosity and surface area, confirming that porosity plays an important role in the adsorption process as also shown by El-Sayed and Bandosz [74]. The highest the percentage of microporosity the better the adsorptive behavior of the carbon towards PCs is.

4 Conclusion

Olive mill wastes, typical residues of olive-oil extraction, are produced in huge quantities in the Mediterranean region. Olive mill wastes represent a serious environmental issue, due to their high organic load and their content in phytotoxic compounds such as PCs; the development of a sustainable approach for their valorization has become an urgent necessity. In this study, an integrated approach for the valorization of olive mill wastes is suggested, it consisted of the simultaneously conversion of a mixture of OS and OMWW into hydrochar via HTC and its subsequent activation using KOH, at two KOH/HC ratios (2 and 4), to produce AC. The results showed that the use of HTC allowed the conversion of both solid and liquid olive mill wastes into HC without the need of a previous drying step, while the activation of the resulting HC allowed the production of ACs with promising textural characteristics and enhanced adsorptive capacities. Comparing between both used KOH/HC ratios (2 and 4), it was shown that the higher specific surface area (964 m^2/g), pore volume (0.51 cm^3/g) and adsorption capacities toward MB (617 mg/g) and iodine (1203 mg/g) were exhibited by carbon activated with KOH at KOH/HC ratio of 2. SEM analysis proved that KOH activation was able to produce AC with important porosity. A shifting of some surface functional groups to different frequencies and a disappearance of other groups after HC activation was also observed. In the second part of the study, batch adsorption tests were carried out to assess the ability of the produced ACs to remove PCs from OMWW. High removal efficiency of PCs was obtained at high pH values with only slight difference between both AC samples. PCs adsorption on AC samples followed the pseudo-second-order model, while the analysis of the equilibrium adsorption data revealed that nonlinear Langmuir and Freundlich isotherm models could both describe the adsorption of OMWW-PCs onto the studied ACs.

The results of the present study revealed that the combination of HTC and KOH activation is an effective method for the valorization of olive mill wastes. This integrated strategy provides a two-fold solution to olive mills, the valorization of both solid and liquid olive mill wastes in one stream and their conversion into high-added-value product as well as the treatment of highly polluting industrial wastewater. Additional studies are, however, still necessary to extend the research to a better understanding of the main mechanisms involved in the adsorption of the different phenolic substances present in complex matrices such as OMWW; this will help to design ACs' properties to be suitable to this application. More focus should also be paid to hydrochar as an emerging adsorbent; optimize the preparation conditions and explore the possibilities of its modification to improve its adsorption capacity towards complex molecules such as PCs.

Declarations

Ethics approval Not applicable.

Competing interests The authors declare no competing interests.

References

1. Pari G, Darmawan S, Prihandoko B (2014) Porous carbon spheres from hydrothermal carbonization and KOH activation on cassava and tapioca flour raw material, Procedia. Environ Sci 20:342–351

2. Enaime G, Ennaciri K, Ounas A, Baçaoui A, Seffen M, Selmi T, Yaacoubi A (2017) Preparation and characterization of activated carbons from olive wastes by physical and chemical activation: application to indigo carmine adsorption, Journal of Materials and Environmental. Science 8:4125–4137

3. Benavente V, Calabuig E, Fullana A (2015) Upgrading of moist agro-industrial wastes by hydrothermal carbonization. J Anal Appl Pyrolysis 113:89–98

4. Gao Y, Chen H, Wang J, Shi T, Yang H, Wang X (2011) Characterization of products from hydrothermal liquefaction and carbonation of biomass model compounds and real biomass. J Fuel Chem Technol 39:893–900

5. Zhu X, Liu Y, Zhou C, Luo G, Zhang S, Chen J (2014) A novel porous carbon derived from hydrothermal carbon for efficient adsorption of tetracycline. Carbon 77:627–636

6. Aljvanieh MG, Geçgel C, Yabala E (2023) Hydrochar synthesis from waste corncob using subcritical water and microwave-assisted carbonization methods and ammonium enrichment of synthesized hydrochars. Environ Res 226:115715

7. Yu Y, Lou X, Wu H (2008) Some recent advances in hydrolysis of biomass in hot-compressed water and its comparisons with other hydrolysis methods. Energy Fuels 22:46–60

8. Teğin IAEYI, Demirel MF (2022) Investigation of the effectiveness of waste nut shell–based hydrochars in water treatment: a model study for the adsorption of methylene blue. Biomass Conv Bioref. https://doi.org/10.1007/s13399-022-02996-y

9. Funke A, Ziegler F (2010) Hydrothermal carbonization of biomass: a summary and discussion of chemical mechanisms for process engineering, Biofuels. Bioprod Biorefining 4:160–177

10. Yabalak E, Eliuz EAE (2022) Green synthesis of walnut shell hydrochar, its antimicrobial activity and mechanism on some pathogens as a natural sanitizer. Food Chem 366:130608

11. Yan W, Acharjee T, Coronella C, Vsquez V (2009) Thermal pretreatment of lignocellulosic biomass, Environ. Prog. Sustain. Energy 28:435–440

12. Enaime G, Baçaoui A, Yaacoubi A, Wichern M, Lübken M (2022) Hydrothermal carbonization of the filter bed remained after filtration of olive mill wastewater on olive stones for biofuel application. Biomass Conv Bioref 12:1237–1247

13. Cao D, Sun Y, Wang G (2007) Direct carbon fuel cell: fundamentals and recent developments. Power Sources 167:250–257

14. Libra J, Ro K, Kammann C, Funke A, Berge N, Neubauer Y, Titirici M, Fühner C, Bens O, Emmerich K (2011) Hydrothermal carbonization of biomass residuals: a comparative review of the chemistry, processes and applications of wet and dry pyrolysis. Biofuels 2:71–81

15. Ighalo JO, Rangabhashiyam S, Dulta K, Umeh CT, Iwuozor KO, Aniagor CO, Eshiemogie SO, Iwuchukwu FU, Igwegbe CA (2022) Recent advances in hydrochar application for the adsorptive removal of wastewater pollutants. Chem Eng Res Des 184:419–456

16. Liu Z, Zhang F (2009) Removal of lead from water using biochars prepared from hydrothermal liquefaction of biomass. J Hazard Mater 167:933–939

17. Falco C, Marco-Lozar J, Salinas-Torres D, Morallon E, Cazorla-Amoros D, Titirici M, Lozano- Castelló D (2013) Tailoring the porosity of chemically activated hydrothermal carbons: influence of the precursor and hydrothermal carbonization temperature. Carbon 62:346–355

18. Shen F, Wang Y, Li L, Zhang K, Smith RL, Qi X (2018) Porous carbonaceous materials from hydrothermal carbonization and KOH activation of corn stover for highly efficient CO_2 capture. Chem Eng Commun. 205:423–431

19. Wu Y, Cao J, Zhao X, Hao Z, Zhuang Q, Zhu J, Wang X, Wei X (2017) Preparation of porous carbons by hydrothermal carbonization and KOH activation of lignite and their performance for electric double layer capacitor. Electrochim Acta 252:397–407

20. Mopoung S, Moonsri P, Palas W, Khumpai S (2015) Characterization and properties of activated carbon prepared from tamarind seeds by KOH activation for Fe(III) adsorption from aqueous solution. Scientific World Journal 2015:9

21. Saad MJ, Chia CH, Zakaria S, Sajab MS, Misran S, Rahman MHA, Chin SX (2019) Physical and chemical properties of the rice straw activated carbon produced from carbonization and KOH activation processes. Sains Malaysiana 48:385–391

22. Gao F, Shao G, Qu J, Lv S, Li Y, Wu M (2015) Tailoring of porous and nitrogen-rich carbons derived from hydrochar for high-performance supercapacitor electrodes. Electrochim Acta 155:201–208

23. Li S, Han K, Li J, Li M, Lu C (2017) Preparation and characterization of super activated carbon produced from gulfweed by KOH activation. Microporous Mesoporous Mater 243:291–300

24. Enaime G, Baçaoui A, Yaacoubi A, Lübken M (2020) Biochar for wastewater treatment—conversion technologies and applications. Appl Sci 10:3492

25. Abid N, Masmoudi MA, Megdiche M, Barakat A, Ellouze M, Chamkha M, Ksibi M, Sayadi S (2022) Biochar from olive mill solid waste as an eco-friendly adsorbent for the removal of polyphenols from olive mill wastewater. Chem Eng Res Des 181:384–398

26. Galiatsatou P, Metaxas M, Arapoglou D, Kasselouri-Rigopoulou V (2002) Treatment of olive mill wastewater with activated carbons from agri-cultural by-products. Waste Manage 22:803–812

27. Ubago-Perez R, Carrasco-Marin F, Fairen-Jimenez D, Moreno-Castilla C (2006) Granular and monolithic activated carbons from KOH-activation of olive stones. Microporous Mesoporous Mater 92:64–70

28. ASTM D4607-94 (2006) Standard Test Method for Determination of Iodine Number of Activated Carbon. ASTM International 100 Barr Harbor Drive: United States

29. Baçaoui A, Yaacoubi A, Dahbi A, Bennouna C, Phan Tan Luu R, Maldonado-Hodar F, Rivera-Utrilla J, Moreno-Castilla C (2001) Optimization of conditions for the preparation of activated carbons from olive- waste cakes. Carbon 39:425–432

30. Singleton V, Rossi J (1965) Colorimetry of total phenolics with phosphomolybdic-phosphotungstic acid reagents. Amer J Enol Viticult 16:144–158

31. Cheng S, Zhang L, Xia H, Peng J, Shu J, Li C, Jiang X, Zhang Q (2017) Adsorption behavior of methylene blue onto waste-derived adsorbent and exhaust gases recycling. RSC Adv 7:27331–27341

32. Ho Y, McKay G (1998) Sorption of dye from aqueous solution by peat. Chem Eng J 70:115–124

33. Langmuir I (1918) The adsorption of gases on plane surfaces of glass, mica and platinum. J Am Chem Soc 40:1361–1403

34. Wang Y, Zhang Y, Li S, Zhong W, Wei W (2018) Enhanced methylene blue adsorption onto activated reed-derived biochar by tannic acid. J Mol Liq 268:658–666

35. Pala M, Kantarli I, Buyukisik H, Yanik J (2014) Hydrothermal carbonization and torrefaction of grape pomace: A comparative evaluation. Bioresour Technol 161:255–262

36. Spagnoli A, Giannakoudakis D, Bashkova S (2017) Adsorption of methylene blue on cashew nutshell-based carbons activated with zinc chloride: the role of surface and structural parameters. J Mol Liq 229:465–471

37. Wang S, Wang K, Liu Q, Gu Y, Luo Z, Cen K, Fransson T (2009) Comparison of the pyrolysis behavior of lignins from different tree species. Biotechnol Adv 27:562–567

38. Chen Z, Chen B, Chiou C (2012) Fast and slow rates of naphthalene sorption to biochars produced at different temperatures. Environ Sci Technol 46:11104–11111

39. Islam M, Tan I, Benhouria A, Asif M, Hameed B (2015) Mesoporous and adsorptive properties of palm date seed activated carbon prepared via sequential hydrothermal carbonization and sodium hydroxide activation. Chem Eng J 270:187–195

40. Javed H, Luong D, Lee C-G, Zhang D, Tour JM, Alvarez P (2018) Efficient removal of bisphenol-A by ultra-high surface area porous activated carbon derived from asphalt. Carbon 140:441–448

41. Titirici M, Thomas A, Yu S, Müller J, Antonietti M (2007) A direct synthesis of mesoporous carbons with bicontinuous pore morphology from crude plant material by hydrothermal carbonization. Chem Mater 19:4205–4212

42. Li W-H, Yue Q-Y, Gao B-Y, Ma Z-H, Li Y-J, Zhao H-X (2011) Preparation and utilization of sludge-based activated carbon for the adsorption of dyes from aqueous solutions. Chem Eng J 171:320–327

43. Chen X, Zhang H, Guo Y, Cao Y, Cheng F (2020) Activation mechanisms on potassium hydroxide enhanced microstructures development of coke powder. Chin J Chem Eng 28:299–306

44. Tan I, Ahmad A, Hameed B (2008) Preparation of activated carbon from coconut husk: optimization study on removal of 2,4,6-trichlorophenol using response surface methodology [j]. J Hazard Mater 153:709–717

45. Guo S, Dong X, Wu T, Shi F, Zhu C (2015) Characteristic evolution of hydrochar from hydrothermal carbonization of corn stalk. J Anal Appl Pyrolysis 116:1–9

46. Erdogan E, Atila B, Mumme J, Reza MT, Toptas A, Elibol M, Yanik J (2015) Characterization of products from hydrothermal carbonization of orange pomace including anaerobic digestibility of process liquor. Bioresour Technol 196:35–42

47. Figueiredo J, Pereira M, Freitas M, Órfão J (1999) Modification of the surface chemistry of activated carbons. Carbon 37:1379–1389

48. de Araújoa TP, Quesadaa HB, Bergamasco R, Vareschinia DT, de Barros MASD (2020) Activated hydrochar produced from brewer's spent grain and its application in the removal of acetaminophen. Biores Technol 310:123399

49. Yu X, Liu S, Lin G, Yang Y, Zhang S, Zhao H, Zheng C, Gao X (2020) KOH-activated hydrochar with engineered porosity as sustainable adsorbent for volatile organic compounds. Colloids Surf A 588:124372

50. Hoekman S, Broch A, Robbins C (2011) Hydrothermal carbonization (HTC) of lignocellulosic biomass. Energy Fuels 25:1802–1810

51. Thommes M, Kaneko K, Neimark A, Olivier J, Rodriguez-Reinoso F, Rouquerol J, Sing K (2015) Physisorption of gases, with special reference to the evaluation of surface area and pore size distribution (IUPAC technical report). Pure Appl Chem 87:1051–1069

52. Stavropoulos G, Zabaniotou A (2005) Production and characterization of activated carbons from olive-seed waste residue. Microporous Mesoporous Mater 82:79–85

53. Shen F, Wang Y, Li L, Zhang K, Jr RS, Qi X (2017) Porous carbonaceous materials from hydrothermal carbonization and KOH activation of corn stover for highly efficient CO_2 capture. Chem Eng Commun 205:423–431

54. Abdel-Ghani N, El-Chaghaby G, ElGammal M, Rawash E (2016) Optimizing the preparation conditions of activated carbons from olive cake using KOH activation. New Carbon Mater 31:492–500

55. Tseng R, Tseng S, Wu F, Hu C, Wang C (2008) Effects of micropore development on the physicochemical properties of KOH-activated carbons. J Chinese Inst Chem Eng 39:37–47

56. Patil B, Kulkarni K (2012) Development of high surface area activated carbon from waste material [j]. Int J Adv Eng Res Stud I:2249–8974

57. El-Hendawy A (2009) An insight into the KOH activation mechanism through the production of microporous activated carbon for the removal of pb^{2+} cations. Appl Surf Sci 255:3723–3730

58. Lu X, Pellechia P, Flora J, Berge N (2013) Influence of reaction time and temperature on product formation and characteristics associated with the hydrothermal carbonization of cellulose. Bioresour Technol 138:180–190

59. Liu MY, Tsang DC, Hu J, Ng KT, Liu T, Lo IM (2008) Adsorption of methylene blue and phenol by wood waste derived activated carbon. J Environ Eng 134:338–345

60. Rodriguez-Reinoso F (2001) Activated carbon and adsorption. Encyclopedia of materials: Science and technology, pp 22–34

61. Roostaei N, Tezel H (2004) Removal of phenol from aqueous solutions by adsorption. J Environ Manage 70:157–164

62. Senol A, Hasdemir M, Hasdemir B, Kurdas I (2017) Adsorptive removal of biophenols from olive mill wastewaters (OMW) by activated carbon: mass transfer, equilibrium and kinetic studies, Asia-Pacific. J Chem Eng 12:128–146

63. Aliakbarian B, Casazza A, Perego P (2015) Kinetic and isotherm modelling of the adsorption of phenolic compounds from olive mill wastewater onto activated carbon. Food Technol Biotechnol 53:207–214

64. Ahmaruzzaman M, Sharma D (2005) Adsorption of phenols from wastewater. J Colloid Interface Sci 287:14–24

65. Stasinakis A, Elia I, Petalas A, Halvadakis C (2008) Removal of total phenols from olive-mill wastewater using an agricultural by-product, olive pomace. J Hazard Mater 160:408–413

66. Laszlo K, Podkoscielny P, Dabrowski A (2003) Heterogeneity of polymer-based active carbons in adsorption of aqueous solutions of phenol and 2,3,4-trichlorophenol. Langmuir 19:5287–5294

67. Michailof C, Stavropoulos GG, Panayiotou C (2008) Enhanced adsorption of phenolic compounds, commonly encountered in olive mill wastewaters, on olive husk derived activated carbons. Biores Technol 99:6400–6408

68. Radovic L, Silva I, Ume J, Menendez J, Leon CL, Scaroni A (1997) An experimental and theoretical study of the adsorption of aromatics possessing electron-withdrawing and electron-donating functional groups by chemically modified activated carbons. Carbon 35:1339–1348

69. Romero-Cano L, Gonzalez-Gutierrez L, Baldenegro-Perez L (2016) Biosorbents prepared from orange peels using instant controlled pressure drop for Cu (II) and phenol removal. Ind Crops Prod 84:344–349

70. Dabrowski A, Podkoscielny P, Hubicki Z, Barczak M (2005) Adsorption of phenolic compounds by activated carbon — a critical review. Chemosphere 58:1049–1070

71. Lawal A, Hassan M, Ahmad Farid M, Yasim-Anuar T, Mohd Yusoff M, Zakaria M, Roslan A, Mokhtar M, Shirai Y (2020) One-step steam pyrolysis for the production of mesoporous biochar from oil palm frond to effectively remove phenol in facultatively treated palm oil mill effluent. Environ. Technol. Innov 18:100730

72. Achak M, Hafidi A, Mandi L, Ouazzani N (2014) Removal of phenolic compounds from olive mill wastewater by adsorption onto wheat bran. Desalin Water Treat 52:2875–2885

73. Malkoc E, Nuhoglu Y, Dundar M (2006) Adsorption of chromium (VI) on pomace—an olive oil industry waste: batch and column studies. J Hazard Mater B 138:142–151

74. El-Sayed Y, Bandosz T (2002) Acetaldehyde adsorption on nitrogen- containing activated carbons. Langmuir 18:3213–3218